Am J Transl Res 2026;18(3):1923-1934
www.ajtr.org /ISSN:1943-8141/AJTR0169254

Original Article

Evaluation of continuous axial stress on tibial fracture healing in canine models using custom external fixator

Yizhe Fan, Xiao Zhang, Zhongyuan Shen, Zhen Han, Chengjian Wei

Department of Orthopedics, The Affiliated Hospital of Nanjing University of Chinese Medicine, Nanjing 210029, Jiangsu, China

Received October 11, 2025; Accepted January 30, 2026; Epub March 15, 2026; Published March 30, 2026

Abstract: Objectives: To investigate the effects of physiologically relevant continuous axial stress on tibial fracture healing in canines using a custom external fixator. Methods: A custom external fixator was developed to apply quantifiable stress. First, maximum axial stress derived from muscle contraction was measured using a film sensor. Subsequently, canine tibial fracture models were established and assigned to non-stress, half-maximum stress, or maximum stress groups. Healing was evaluated via radiography, micro-computed tomography (Micro-CT), biomechanical testing, Western Blot, and Real-time Polymerase Chain Reaction (PCR). Results: The maximum physiological axial stress was measured at 460 g. Compared with maximum stress and non-stress groups, the half-maximum stress group exhibited superior fracture healing, evidenced by increased callus formation and bone volume ratio (BV/TV) in X-ray and micro-CT analyses. Biomechanical testing demonstrated significantly higher ultimate strength in the half-maximum group. Molecular analyses further supported these observations, showing sustained upregulation of Runt-related transcription factor 2 (RUNX2) and Type I Collagen (COL-1) expression in the half-maximum group. Conclusions: Muscle contraction generates a maximum axial stress of approximately 460 g at canine tibial fracture sites. Continuous application of half the maximum axial stress significantly enhances fracture healing compared to both maximum stress and non-stress conditions.

Keywords: Continuous axial stress, tibial fracture, healing, canine, external fixator

Introduction

Each year, approximately 16 million fractures occur in the United States [1], and non-union occurs in approximately 2% of these cases [2]. This number can reach 20% when it comes to diaphyseal fractures [3]. Non-union represents a chronic medical condition not only causing long-term pain and function loss but also potentially brings psychological and economic distress upon the individual [4]. Combining estimated medical expenses with loss of potential earnings, the financial implications can reach £79,000 per non-union case [3, 5]. More importantly, non-union leads to chronic pain and loss of limb function, often causing muscle atrophy and joint stiffness. Therefore, it is necessary to find an effective method to prevent non-union and promote fracture healing.

Fracture healing is a distinctive process leading to bone regeneration, which contains four phases: fracture hematoma and inflammatory response; cartilage formation; cartilage removal, calcification; and finally chronic bone remodeling [6]. Both mechanical environment and biological environment are critical for fracture healing [7, 8]. As recently as four decades ago, Wolff pointed out that bone function and structure can be influenced by mechanical stress stimulation [9]. Specifically, axial interfragmentary movement has been identified as a potent stimulator of secondary bone healing, promoting cartilaginous callus formation and subsequent ossification [10]. Lack of mechanical stress can lead to the degeneration of bone microstructure and occurrence of bone loss [11]. Prolonged bed rest, lack of exercise and weightlessness in space are typical situations in the absence of mechanical stress and can lead to osteoporosis [11, 12]. Conversely, behaviors such as exercise can improve mechanical load and reverse these negative effects and restore bone mass [13].

https://doi.org/10.62347/JTFO9352

Clinically, treatment options for tibial fractures primarily include intramedullary nailing, plate osteosynthesis, and external fixation [14]. While rigid internal fixation provides mechanical stability, it may lead to "stress shielding", where the implant bears the load and deprives the bone of necessary mechanical stimulation, potentially delaying healing [15]. Cast fixation is currently the most common conservative treatment for fracture. However, protracted immobilisation in a cast brings stiffness and inconvenience, while the lack of stress on the broken end delays healing [16]. In China, there is a traditional way of conservatively treating fracture named splint fixation. On the one hand, splint fixation leads to a stabilization of the fracture end, which has previously been demonstrated by biomechanics [17]. On the other hand, patients can perform functional exercise with external fixation from a splint. Exercise brings axial stress through muscle contraction. However, the efficacy of such dynamic loading depends heavily on stress magnitude. While previous studies suggest that axial micromotion enhances callus formation [18], excessive motion can cause instability, whereas insufficient motion fails to stimulate osteogenesis. The concrete numerical magnitude of axial stress has not been researched. Our study was designed for a preliminary investigation of axial stress.

In our studies, we designed a novel canine-specific external fixator based on hindlimb anatomy. This custom device integrates three key functions: (1) maintaining anatomical reduction, (2) applying quantifiable continuous axial stress, and (3) real-time stress monitoring. Prior to main experiments, we first determined the maximum axial stress at fracture sites derived from muscle contraction through pre-experimentation. Using the measurements, we established three experimental groups: non-stress group, half the maximum axial stress group, the maximum axial stress group. Fracture healing progression was comprehensively assessed through micro-computed tomography (μCT), biomechanical testing, and other measures at predetermined timepoints. This investigation specifically aimed to address two critical questions: first, whether physiologically-relevant axial stress derived from simulated muscle contraction enhances fracture healing; and second, which specific axial stress magnitude optimally promotes fracture healing.

Materials and methods

Experimental animals

All experiments involving animals followed international regulations for the care and use of laboratory animals and were approved by the Animal Care and Use Committee of Nanjing University of Chinese Medicine (Approval No. AUC221103). A total of 17 adult male beagle dogs, weighing 10 kg-15 kg, were obtained from Taisite Biotechnology Co., Ltd. (China) under the animal production license number SCYK (Su) 2021-0010. Hind limb bone and joint diseases were ruled out by stifle and hip radiographs.

Prior to the experiment, all animals were allowed a 3-day acclimatization period. They were housed in individual ventilated cages under controlled environmental conditions, with a temperature of 23±3°C, a relative humidity of 40%-70%, and a standard 12-h light/12-h dark cycle. Throughout the study, the animals had a free access to standard diet and water.

External fixator design and construction

The external fixators were formed by resins and stainless steel (**Figure 1A**). Both sides of fixators were fixing clamps and fixing blocks, they had a few holes where K-wires could go through. K-wires could be fixed to external fixators by locking the fixing screw simultaneously. Fixing clamps were connected with a pressure sensor via a tie rod. There were also a nut and a spring on the rod (**Figure 1B**). By rotating the nut, the spring could be compressed and apply stress to fracture end. The stress signals received by the sensor on the rod could be read out using a supporting data display (**Figure 1C**).

Transverse tibial fracture model construction

Experimental animals were anesthetized with 3 mg/kg of pentobarbital and all the modeling procedures were operated by three researchers with orthopedic surgery background. In brief, through the medial approach, the skin and subcutaneous tissue of left middle tibia was cut layer-by-layer to expose the middle tibia. Based on the location of the external fixator holes, three K-wires (60 mm length, 1.5 mm gauge) were introduced perpendicular to the long axis of the tibia at the proximal and

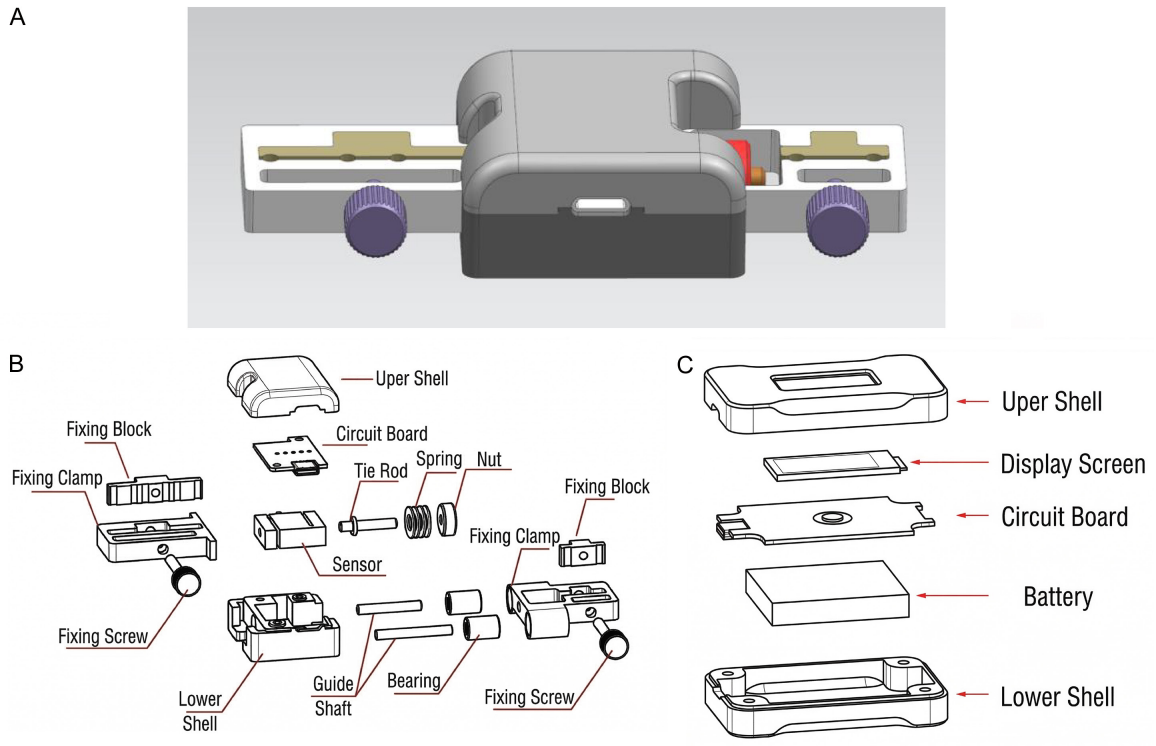

Figure 1. Custom external fixator and data display. A. Overall appearance of custom external fixator. B. Internal structure of custom external fixator. C. Internal structure of data display.

distal end of fracture site. Then under continuous saline irrigation, a 2 mm oscillating micro saw (provided by Waston Medical Appliance, China) was used to make a transverse fracture of the middle tibia. An X-ray radiograph was performed to ensure the modeling success. To eliminate uncontrolled physiological axial stress generated by the triceps surae muscle group, a standard Achilles tenotomy was performed. By severing the tendon, the mechanical transmission of muscle contraction forces to the calcaneus was disrupted, thereby minimizing intrinsic axial loading on the tibial shaft. This procedure, combined with the use of the suspension wheelchair, ensured that the mechanical environment at the fracture site was determined solely by the external fixator. To assure the consistency of the results, the length of K-wires was kept equal on both tibial sides. Meanwhile, a distance of 4 cm was kept between two external fixators when they were attached to K-wires. Suture incision occurred layer-by-layer. The right tibia was treated with the same method. Following the operation, 300,000 units penicillin were injected for 3 consecutive days to prevent infection.

Axial stress assay of fracture end

Axial stress assay of fracture end prior to the main fracture healing experiment, 2 canines were randomly selected specifically for a preliminary study to measure the physiological axial stress at the fracture end. A total of 3 tibias from these two animals were used for sensor implantation and the assay was repeated three times (one canine underwent bilateral testing, and the other underwent unilateral testing). Fracture modeling was carried out using the same method as described above and the Achilles tendon was preserved. A film stress sensor (Leanstar Electronic Technology, China) was inserted into fracture gap. In order to determine the position of sensor, a 2 mm thick sterile iron sheet was attached to the sensor with silk suture. After confirming the position of sensor with fluoroscopy, the Canines were placed belly down on a suspended bed with four legs hanging free and feet off the ground. After awakening from anesthesia and removing the springs on the external fixators, the Canines were allowed to be active for 24 h and stress data were recorded by the sensor at

2-min intervals. The average of the three maxima was taken as the maximum axial stress.

The relationship between axial stress and readings of external fixators

Considering that the K-wires could become curved while external fixators applied axial stress, readings of external fixators were higher than actual axial stress. We conducted a pre-experiment to test the relationship between axial stress and readings of external fixators. The result showed that a linear correlation was observed between the readings of external fixators and the axial stress at fracture ends within a certain range [19]. We maintained the readings of the two external fixators on both sides equally and rotated the nut according to the pre-experiment results until readings of external fixators were acquired.

Grouping of animals

The grouping rationale was based on the maximum physiological axial stress (460 g) determined in our pre-experiment. To identify the optimal mechanical environment for fracture healing, we established a stress gradient relative to this physiological limit: (1) Non-stress group (Group A, 0 g), serving as a baseline control established by casting and Achilles tenotomy; (2) Half-maximum axial stress group (Group B, 230 g), representing a moderate loading condition; and (3) Maximum axial stress group (Group C, 460 g), simulating the full physiological load.

Following 3 days of adaptive feeding, fracture modeling commenced (Day 0). A total of 15 canines were assigned to these conditions. Specifically, 6 canines were assigned to the Non-stress type (Type IV), where fractures were stabilized by plaster casts (Xiemin Medical Surgical Dressing Factory, China) with knee and ankle fixation. The remaining 9 canines underwent external fixation with different continuous axial stress configurations: Type I applied maximum stress to both tibias (n=3); Type II applied half-maximum stress to both tibias (n=3); and Type III applied maximum stress to the left tibia and half-maximum stress to the right tibia (n=3). All animals were placed in custom 3D-printed wheelchairs (Patent No. 202222052214.6) to prevent weight-bearing while allowing forelimb mobility. At predetermined time points (2, 4, and 8 weeks), animals were euthanized for sample collection. Euthanasia was performed by a lethal intravenous overdose of propofol (1 g/kg) administered via the cephalic vein of the forelimb. Bilateral tibias were harvested. Considering that canine hyperactivity could cause fracture displacement under cast immobilization, 3 samples with optimal alignment were selected from the total 4 samples available in the Non-stress group at each time point.

X-ray examinations

X-ray examination was performed using a standard clinical digital system (R-30H, Shimadzu, Tokyo, Japan). The X-ray tube was set at 40 kV, 10 mA, 0.06 s and the distance of the X-ray tube to fracture samples was 40 cm. The bone healing was assessed according to the Lane-Sandhu X-ray scoring standard (**Table 1**) [20]. The average scores given by two attending orthopaedic surgeons with more than 8 years clinical experience was considered as the final score.

Micro-CT scans

Fracture samples were analyzed by micro-CT (Hiscan XM micro-CT, Hiscan Information Technology, China). Scans were acquired using the following: 80 kV, 100 μA, 50 ms integration time and scanning resolution was 25 μm. Image processing and data evaluation were performed using software self-developed by Hiscan. Volumes of interest (VOIs) were determined for Micro-CT analysis and covered the whole fracture callus. The relative bone volume (bone volume/total volume, BV/TV), trabecular bone thickness (Tb. Th), the amount of trabecular bone (Tb. N) and trabecular bone separation (Tb. Sp) of fracture samples were detected.

Biomechanical testing

Tibias of canines sacrificed were subjected to a 3-point-bending test using a materials testing machine (HZ-1009B, Dongguan Lixian Instrument Technology, Dongguan, China) as published before [21]. The span between the two lower supports was 10 cm and a 1-mm-thick blade was implemented on the top surface of callus tissue (**Figure 2**). The load was applied at a speed of 2 mm/min until the fracture sam-

Table 1. Lane-Sandhu X-ray scoring standard

Variable	Indicators	Score
Bone formation	No bone formation	0
	New bone formation accounts for less than 25%	1
	New bone formation accounts for 25%-50%	2
	New bone formation accounts for 50%-75%	3
	New bone formation accounts for more than 75%	4
Bone union	Fracture line is clear	0
	Fracture line is blurred	2
	Fracture line is obliterated	4
Medullary cavity remodeling	No remodeling	0
	Medullary cavity partial remodeling	2
	Cortical bone formation after medullary cavity remodeling	4

Figure 2. Biomechanical testing.

ple was brought to ultimate failure. Ultimate strength was calculated at the maximum load before failure.

Real-time PCR

Total RNA from callus was extracted by using TRIzol reagent (Invitrogen, Carlsbad, CA, USA) according to the manufacturer's instructions, and was synthesized to cDNA by reverse transcription (cDNA synthesis kit, TaKaRa, Tokyo, Japan). Power SYBR Green PCR Master Mix (Applied Biosystems, Foster City, CA, USA) was used for real-time PCR. The mRNA levels of RUNX2 and COL-1 were analyzed using primer sequences listed in **Table 2**. Real-time PCR was performed using Premix Ex Taq SYBR-Green PCR (TaKaRa Biotechnology, Tokyo, Japan) according to the manufacturer's instructions on an ABI PRISM 7300 (Applied Biosystems, Foster City, CA, USA). The mRNA level of individual genes was normalized to GAPDH and calculated by the $2^{-\Delta\Delta CT}$ data analysis method.

Western blotting

Total proteins were obtained by adding RIPA lysate, and the protein concentration were measured in accordance with the instructions for the preparation of the BSA standard curve. According to the determination of protein concentration and the volume of the sample, electrophoresis and membrane transfer were performed with BSA. The corresponding primary antibody (1:1,000) was added, followed by incubation with secondary antibody and the protein was quantified.

Statistical analysis

Statistical analyses were performed using SPSS 23.0 software (IBM, Armonk, NY, USA). Data are presented as mean ± standard deviation (SD). The normality of the data distribution was verified using the Shapiro-Wilk test. For comparisons among the three experimental groups (Non-stress, Half-maximum stress, and Maximum stress), One-way Analysis of Variance (ANOVA) was employed. When the ANOVA indicated significant differences, Fisher's Least Significant Difference (LSD) post hoc test was used for pairwise comparisons. A p-value < 0.05 was considered statistically.

Results

The axial stress within 24 h

The progress of fracture modeling is shown in **Figure 3A** and **3B**. Successful establishment of the canine model of tibial fracture was confirmed by using X-ray (**Figure 3C**, **3D**). The film stress sensor was inserted into fracture gap

Table 2. Nucleotide sequences of primers used for Real-time PCR amplification

Target gene	Forward primer	Reverse primer
RUNX2	ATGGCACGACACCACGAC	TCATCTGGCTCAGATAGGAGGA
COL-1	GAGGGCCAAGACGAAGACATC	CAGATCACGTCATCGCACAAC
GAPDH	TCAACAGCAACTCCCACTCTT	TTGAGGGTGCAGCGAACTT

with the reading zeroed and location was identified by X-ray (**Figure 3E**, **3F**). The maximum axial stress data of the three tibias within 24 h were 426 g, 481 g and 473 g. The average of the three maxima was 460 g and this value was taken as the maximum axial stress.

The relationship between axial stress and readings of external fixators

According to our pre-experimental results [19], when the readings of two external fixators are both about 1,300 g, the continuous axial stress at the fracture end could reach the maximum value = 460 g (**Figure 4A**). By the same reasoning, when the readings are both about 750 g, external fixators can apply half the maximum axial stress to the fracture end (**Figure 4B**). So we adjusted the readings of the external fixators to the ideal value, placed the canines in our 3D printed wheelchairs, and proceeded with the subsequent experiments (**Figure 4C**).

X-ray evaluation and lane-Sandhu scoring

X-ray at all 3 time-points revealed that the alignment of transverse fracture was good. Two weeks following the operation, the fracture gap was noticeable and the callus was not easily observed in all three groups. At 4 weeks, a wide variety of callus was visible around the broken end and the fracture gap became narrowed among the maximum axial stress group and half the maximum axial stress group. In contrast, there was still no clear sign of new bone tissue regeneration in the non-stress group (**Figure 5A**). When it came to 8 weeks, the callus size in all groups was significant, and there was a more evident increase in callus formation in group B and group C compared to group A (**Figure 5B**).

Lane-Sandhu radiographic scoring results are shown in **Table 3**. There was no prominent bone formation at 2 weeks and all groups scored 0. However, at 4 weeks and 8 weeks, group A had the lowest score compared to the other 2 groups ($P<0.05$). Meanwhile, there was a certain gap between group B and group C, albeit without being statistically significant ($P>0.05$).

Micro-CT results

Following micro-CT scanning, we first created three dimensional reconstructions to evaluate tibial geometry and fracture healing crudely. After 2 weeks, only a trace amount of bone tissue could be observed around the broken end and was invisible inside the defect in all three groups. Four weeks post-operation, an increase in newly formed bone could be found in all three groups. At 8 weeks, the fracture line became relatively blurred. Meanwhile, in the maximum axial stress group and half the maximum axial stress group, the trabecular bones were thicker and denser, with better continuity (**Figure 6**). Then we performed a more nuanced analysis on the quantity of newly formed bone. Compared with group B and group C, the non-stress group had the lowest BV/TV at 4 and 8 weeks, as well as the highest Tb. The same was true at 8 weeks. Further, at 4 weeks, the half the maximum axial stress group still had the highest BV/TV compared with other groups, and this difference was statistically significant ($P<0.05$). These results showed some numerical differences, but they are not statistically significant ($P>0.05$) (**Table 4**).

Biomechanical testing results

The results of three-point bending test (biomechanical testing) of the tibia are shown in **Table 5**. At 2 weeks, there were no significant signs of healing and sufficient mechanical stability at the fracture end in any of the groups, so we skipped the testing. At 4 and 8 weeks, statistically significantly highest forces were obtained in half the maximum axial stress group compared to two other groups. At the same time, the maximum axial stress group also had higher forces than the non-stress group, although it did not reach half the maximum axial stress group.

Western blot and real time PCR

Western Blot and Real time PCR were used to detect RUNX2, COL-1 protein and gene expression in fracture callus tissues at 2, 4 and 8

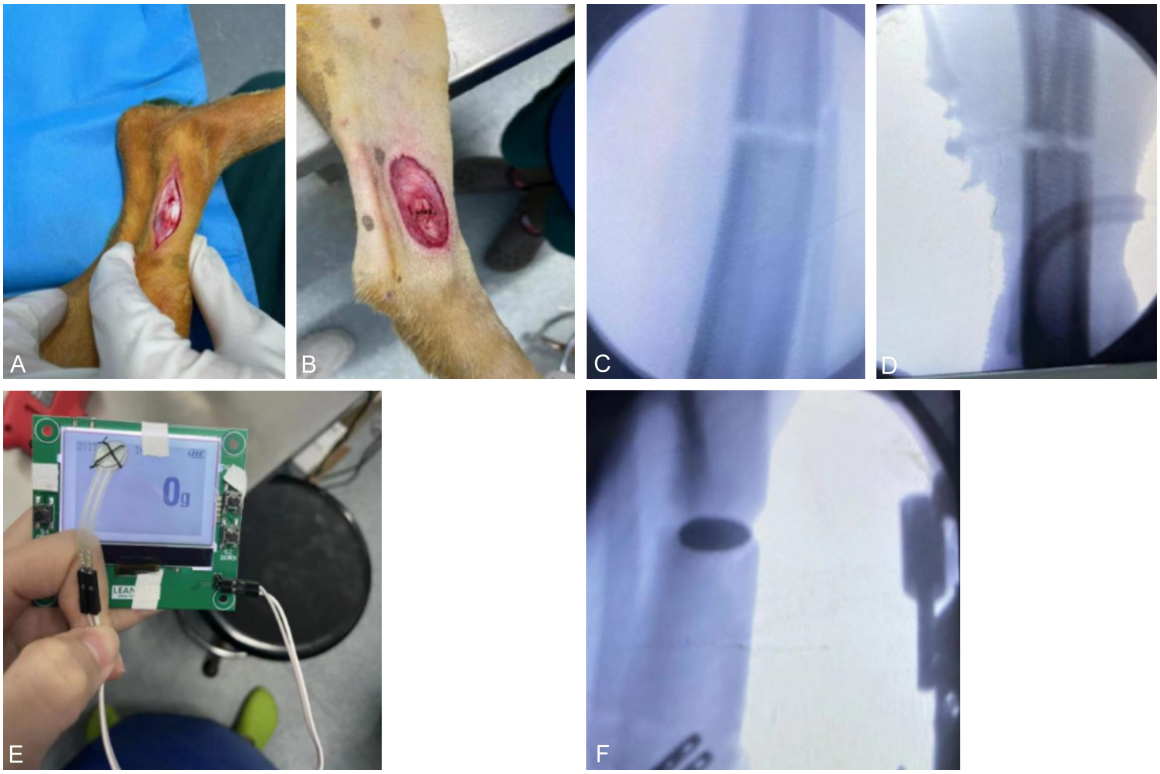

Figure 3. Fracture modeling and stress measurement. A, B. Progress of fracture modeling. C, D. Verify the success of the fracture model by X-ray. E. Film stress sensor with reading zeroed. F. X-ray showed satisfactory location of film stress sensor.

Figure 4. The method of applying continuous axial stress. A. The readings were adjusted to 1,300 g and the external fixators applied the maximum axial stress to the fracture end. B. The readings were adjusted to 750 g and the external fixators applied the half maximum axial stress to the fracture end. C. The use of 3D printed wheelchair.

weeks post-fracture. The results revealed that the half maximum axial stress group consistently exhibited the highest levels of RUNX2 and COL-1 protein and gene expression at all time points. The maximum axial stress group demonstrated intermediate levels of RUNX2 and COL-1 expression, suggesting that while mechanical stimulation promotes osteogenesis, excessive loading may not further enhance the expression of these markers and could potentially impede the healing process. In contrast, the non-stress group consistently dis-

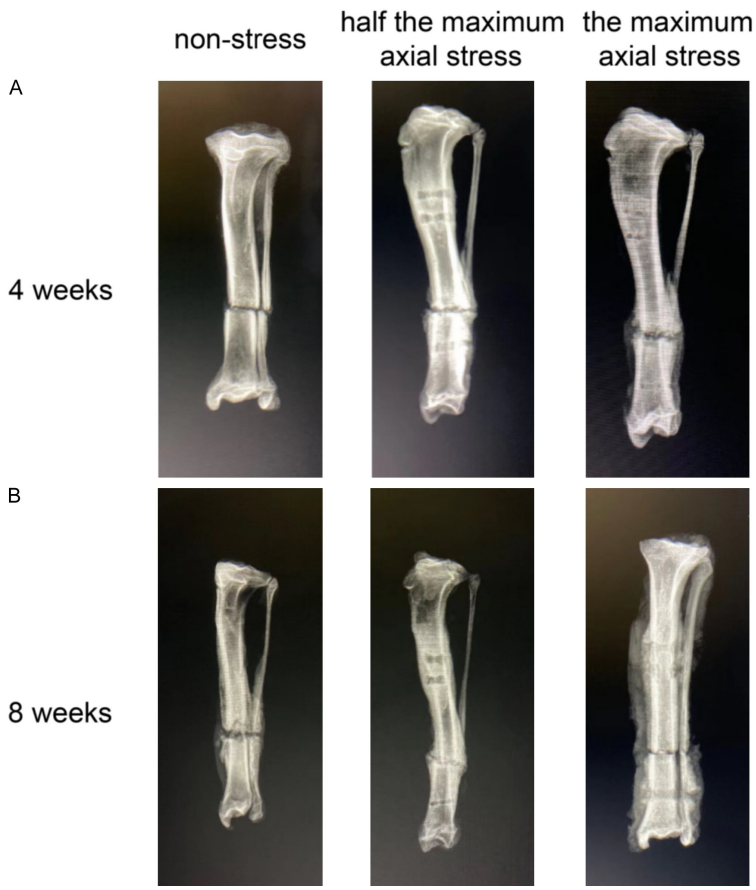

Figure 5. X-ray images of fracture healing. A. Representative X-ray images of 3 groups at 4 weeks. B. Representative X-ray images of 3 groups at 8 weeks.

Table 3. Lane-Sandhu scoring results

Group	2 weeks	4 weeks	8 weeks
Non-stress group	0	0.3±0.6	2.3±0.6
Half maximum axial stress group	0	0.8±0.4*	3.3±0.5*
Maximum axial stress group	0	0.6±0.6*	3.2±0.6*

*$P<0.05$ vs. Non-stress groups. Data are presented as mean ± SD. Statistical significance was determined using One-way ANOVA followed by LSD post hoc test.

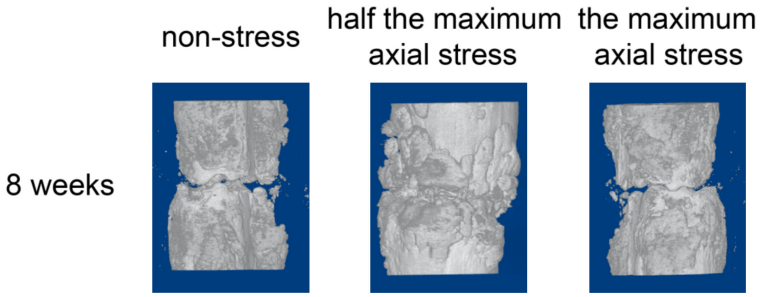

Figure 6. Three dimensional reconstructions image of fracture healing at 8 weeks.

played the lowest levels of RUNX2 and COL-1 expression (**Figure 7A-C**).

Discussion

Axial stress stimulation is the most frequent and common factor affecting long bone fracture healing. It contains several parameters: magnitude of the stress, frequency of the stress and intervention time. In recent years, there have been many studies on the effects of mechanical stress on fracture healing, but most have focused on intermittent stress and have some limitations. Leung [22] applied high-frequency (10-30 Hz) and low-intensity (amplitude of 0.3 g gravitational acceleration) intermittent stress which can effectively accelerate callus formation, thereby promoting fracture healing. However, there is currently no clear conclusion regarding the specific effects of different combinations of stress magnitude and frequency on fracture healing. Goodship [23] applied regular periodic passive stimulation to the fracture end of experimental animals using external fixation. However, after surgery, the animals immediately began weight-bearing walking. This experimental design led to a significant discrepancy between the actual stress experienced at the fracture site and the preset values, thereby affecting the accuracy of the experimental results. As a whole, this approach cannot necessarily be accepted by patients and is difficult and complex to move from laboratory to clinic.

In our experiment, we first used a film stress sensor to mea-

Table 4. Results of BV/TV, TbSp, TbTh and TbN in the region of interest

Group	BV/TV		
	2 weeks	4 weeks	8 weeks
Non-stress group	0.103±0.063	0.131±0.053	0.165±0.043
Half maximum axial stress group	0.226±0.074	0.408±0.052*	0.490±0.078*
Maximum axial stress group	0.211±0.064	0.263±0.008*,#	0.379±0.076*
Group	Tb.Th (mm)		
	2 weeks	4 weeks	8 weeks
Non-stress group	0.209±0.016	0.240±0.072	0.331±0.102
Half maximum axial stress group	0.385±0.217	0.367±0.044	0.561±0.036*
Maximum axial stress group	0.328±0.033	0.346±0.025	0.500±0.133
Group	Tb.N (1/mm)		
	2 weeks	4 weeks	8 weeks
Non-stress group	0.659±0.097	0.537±0.238	0.810±0.302
Half maximum axial stress group	0.750±0.062	0.767±0.165	1.054±0.123
Maximum axial stress group	0.633±0.222	0.578±0.151	0.908±0.402
Group	Tb.Sp (mm)		
	2 weeks	4 weeks	8 weeks
Non-stress group	1.192±0.115	1.781±0.187	1.779±0.233
Half maximum axial stress group	1.099±0.175	0.787±0.260*	0.748±0.105*
Maximum axial stress group	1.312±0.279	1.431±0.493	0.893±0.390*

*P<0.05 vs. Non-stress group; #P<0.05 vs. Half maximum axial stress group. Data are presented as mean ± SD. Statistical significance was determined using One-way ANOVA followed by LSD post hoc test.

Table 5. Three-point bending test results

Group	4 weeks	8 weeks
Non-stress group	173±51.11	305±183.35
Half maximum axial stress group	543±123.27*	893±390.69*
Maximum axial stress group	377±144.01*,#	506±236.36*,#

*P<0.05 vs. Non-stress group; #P<0.05 vs. Half maximum axial stress group. Data are presented as mean ± SD. Statistical significance was determined using One-way ANOVA followed by LSD post hoc test.

sure the maximum axial stress of the canine tibia derived from muscle contraction at approximately 460 g, a result that has not been reported in previous studies. Then we applied different levels of continuous axial stress to the fracture end through our custom external fixator. Combining the results of experiments in radiological and biomechanical results at different time points, half the maximum axial stress group had the best outcome of fracture healing. This finding aligns with the "optimal strain theory" supported by recent studies. For instance, Lv [24] demonstrated that optimizing the fixation stiffness to allow for moderate interfragmentary motion significantly enhances cartilage-to-bone transformation. Similarly, increasing evidence suggests that moderate mechanical loading creates a favorable immune microenvironment for osteogenesis. Molecular biology studies also show similar affects. RUNX2, a transcription factor essential for osteoblast differentiation [25], showed a significant upregulation in the half maximal axial stress group compared to the other groups. Similarly, COL-1, a major extracellular matrix protein in bone, was also markedly elevated in this group, indicating enhanced osteogenic activity and matrix formation [26]. In contrast, the non-stress group consistently showed the lowest levels of RUNX2 and COL-1 expression, underscoring the importance of mechanical stimuli in fracture healing. Results in the maximal axial stress group were at a moderate level, suggesting that while mechanical stimulation promotes osteogenesis, excessive loading may not further enhance the expression of these markers and could potentially hinder the healing process. This result is consistent with the findings of J. Barcik [27], who reported that lower interfragmentary strains (around 2.5%) maximize the density of repair tissue within the fracture gap, whereas higher strain magnitudes significantly shift the

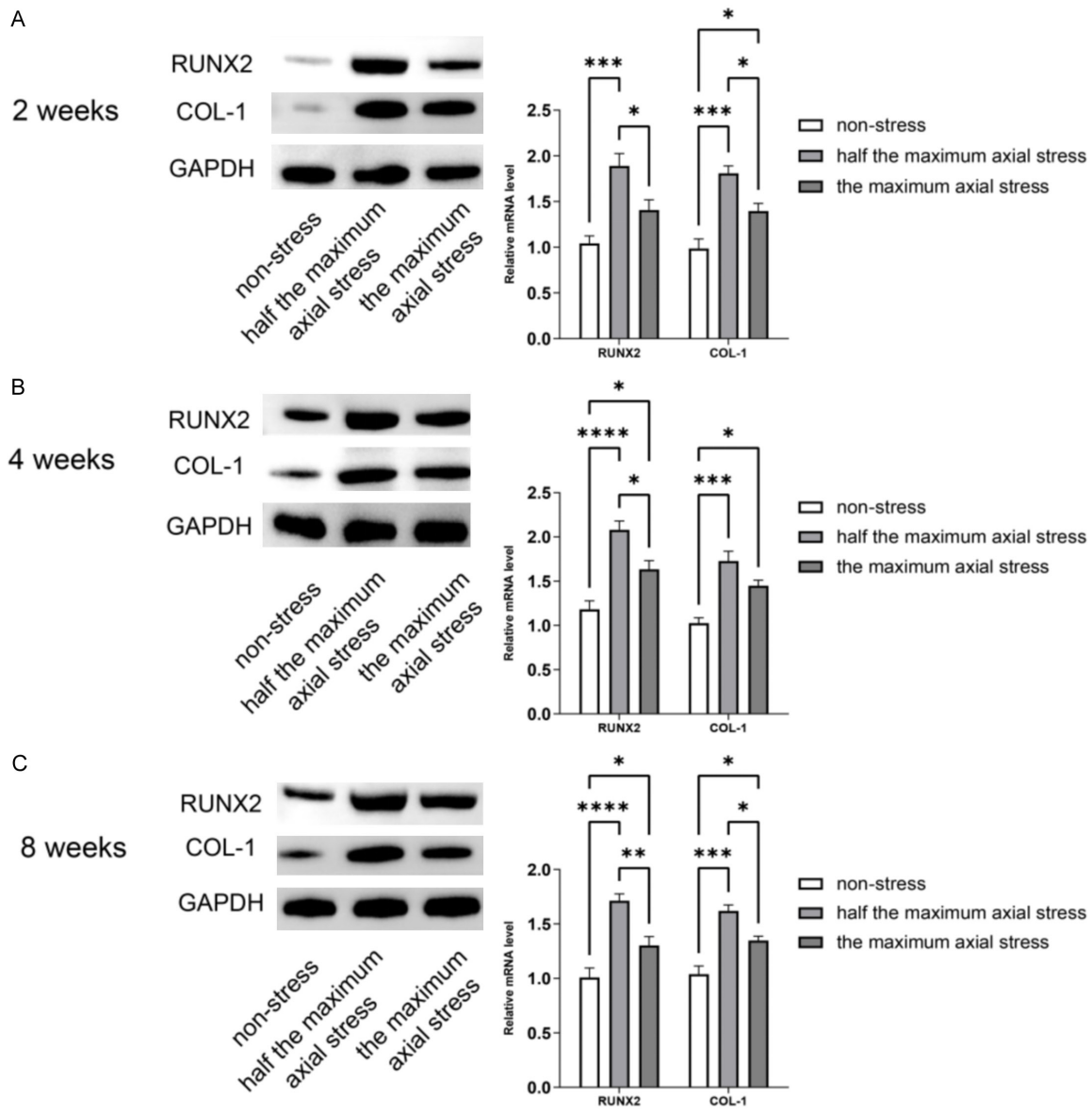

Figure 7. Osteogenesis-related proteins and mRNA expression of 3 groups. A. Typical protein bands and relative gene expression of RUNX2 and COL-1 at 2 weeks. B. Typical protein bands and relative gene expression of RUNX2 and COL-1 at 4 weeks. C. Typical protein bands and relative gene expression of RUNX2 and COL-1 at 8 weeks. *P<0.05 vs. half maximum axial stress group; **P<0.01 vs. half maximum axial stress group; ***P<0.001 vs. half maximum axial stress group; ****P<0.0001 vs. half maximum axial stress group.

healing response toward external periosteal callus formation. This was also in line with the results of other studies [28].

Our study identifies several limitations in existing research methodologies and proposes corresponding optimizations. Firstly, our custom external fixator used in the experimental process demonstrates several advantages: (1) Specifically designed for animal fracture models, it enables real-time monitoring and adjustment of fracture end stress. The digital display of fracture end stress allows for immediate and objective assessment of pressure changes, with simple adjustment mechanisms through rotating nuts, providing a convenient and reliable experimental apparatus for animal studies. (2) The display unit is powered by rechargeable batteries, eliminating the need for external power cords. It can be connected to the measurement device via a data cable and attached to the experimental animal, facilitating experi-

mental procedures. (3) The compact and lightweight design of our custom external fixator minimizes interference with canine daily activities. (4) The simplified fixation mechanism of our device reduces modeling time, decreases operational difficulty, and minimizes harm to experimental animals. (5) Beyond canine applications, this device is adaptable for research on other similarly sized animals, such as rabbits, goats, and rats. Meanwhile, our study implements measures to avoid additional stress interference. These include placing dogs in 3D printed wheelchairs and performing Achilles tendon resection to eliminate the animal's intrinsic stress. These approaches effectively minimize additional stress on the fracture site caused by self-loading, thereby reducing experimental errors to the greatest extent possible.

However, our custom external fixator also presents several limitations during application: (1) The device requires fixation using three K-wires that penetrate the bone shaft. The prolonged presence of these K-wires in vivo poses a risk of infection. To mitigate this issue, we implemented daily wound dressing changes and alcohol application at the pin insertion sites, which proved to be somewhat effective in preventing infections. (2) The device is susceptible to damage during experimental procedures. Nevertheless, its easy replacement and convenient data adjustment features allow for prompt troubleshooting and maintenance. (3) Regarding the plaster cast group, in addition to the Achilles tendon resection, the transarticular plaster fixation was employed to prevent joint movement-induced stress. However, prolonged plaster fixation cannot completely eliminate stress at the fracture gap, representing an area that requires improvement in the experimental design.

Conclusion

Our study unveils that muscle contraction generates maximum axial stress of 460 g at canine tibial fracture sites. Our findings demonstrate that continuous half maximum axial stress (230 g) significantly enhances fracture healing compared to both the maximum axial stress and non-stress conditions. This provides valuable inspiration for our further investigation into splint fixation.

Acknowledgements

The current work was supported by the National Nature Science Foundation of China (No. 81973872); Jiangsu Provincial Medical Key Discipline (Laboratory) Cultivation Unit (No. JSDW202252); Postgraduate Research & Practice Innovation Program of Jiangsu Province (No. SJCX24_0960).

Disclosure of conflict of interest

None.

Address correspondence to: Dr. Chengjian Wei, Department of Orthopedics, The Affiliated Hospital of Nanjing University of Chinese Medicine, No. 155, Hanzhong Road, Qinhuai District, Nanjing 210029, Jiangsu, China. Tel: +86-013306195877; E-mail: drweichengjiantcm@163.com

References

[1] Hadjiargyrou M and O'Keefe RJ. The convergence of fracture repair and stem cells: interplay of genes, aging, environmental factors and disease. J Bone Miner Res 2014; 29: 2307-2322.

[2] Mills LA, Aitken SA and Simpson AHRW. The risk of non-union per fracture: current myths and revised figures from a population of over 4 million adults. Acta Orthop 2017; 88: 434-439.

[3] Nicholson JA, Makaram N, Simpson A and Keating JF. Fracture nonunion in long bones: a literature review of risk factors and surgical management. Injury 2021; 52 Suppl 2: S3-S11.

[4] Wildemann B, Ignatius A, Leung F, Taitsman LA, Smith RM, Pesántez R, Stoddart MJ, Richards RG and Jupiter JB. Non-union bone fractures. Nat Rev Dis Primers 2021; 7: 57.

[5] Patil S and Montgomery R. Management of complex tibial and femoral nonunion using the Ilizarov technique, and its cost implications. J Bone Joint Surg Br 2006; 88: 928-932.

[6] Saul D and Khosla S. Fracture healing in the setting of endocrine diseases, aging, and cellular senescence. Endocr Rev 2022; 43: 984-1002.

[7] Wähnert D, Greiner J, Brianza S, Kaltschmidt C, Vordemvenne T and Kaltschmidt B. Strategies to improve bone healing: innovative surgical implants meet nano-/micro-topography of bone scaffolds. Biomedicines 2021; 9: 746.

[8] Hu J, Peng Y, Li J, Li M, Xiong Y, Xiao J, Zhang L and Tang P. Spatial bridge locking fixator versus traditional locking plates in treating AO/

OTA 32-A3.2 fracture: finite element analysis and biomechanical evaluation. Orthop Surg 2022; 14: 1638-1648.
[9] Wolf JW Jr, White AA 3rd, Panjabi MM and Southwick WO. Comparison of cyclic loading versus constant compression in the treatment of long-bone fractures in rabbits. J Bone Joint Surg Am 1981; 63: 805-810.
[10] Han Z, Wu J, Deng G, Bi C, Wang J and Wang Q. Axial micromotion locking plate construct can promote faster and stronger bone healing in an ovine osteotomy model. Front Bioeng Biotechnol 2021; 8: 593448.
[11] Wang K, Wang Y, Hu Z, Zhang L, Li G, Dang L, Tan Y, Cao X, Shi F, Zhang S and Zhang G. Bone-targeted lncRNA OGRU alleviates unloading-induced bone loss via miR-320-3p/Hoxa10 axis. Cell Death Dis 2020; 11: 382.
[12] Ragnarsson KT. Bone loss and fractures in limbs paralyzed by spinal cord injury: prevention, diagnosis, and treatment. J Spinal Cord Med 2015; 38: 10-12.
[13] Suniaga S, Rolvien T, Vom Scheidt A, Fiedler IAK, Bale HA, Huysseune A, Witten PE, Amling M and Busse B. Increased mechanical loading through controlled swimming exercise induces bone formation and mineralization in adult zebrafish. Sci Rep 2018; 8: 3646.
[14] Raju K, Smith TO, Hing CB, Solan MC and Nielsen DM. Surgical versus conservative interventions for treating tibial shaft fractures in adults. The Cochrane Database of Systematic Reviews 2018; 2018: CD011095.
[15] Beeharry MW and Ahmad B. Principles of fracture healing and fixation: a literature review. Cureus 2024; 16: e76250.
[16] Hsieh YF and Turner CH. Effects of loading frequency on mechanically induced bone formation. J Bone Miner Res 2001; 16: 918-924.
[17] Hoare CP, Dickson DR, Armstrong DJ, Nuttall D and Watts AC. Internal fixation for treating distal radius fractures in adults. The Cochrane Database of Systematic Reviews 2017; 2017: CD011213.
[18] Rechter GR, Anthony RT, Rennard J, Kellam JF and Warner SJ. The impact of early axial interfragmentary motion on the fracture healing environment: a scoping review. Injury 2024; 55: 111917.
[19] Hua Z, Wang JW, Lu ZF, Ma JW and Yin H. The biomechanical analysis of three-dimensional distal radius fracture model with different fixed splints. Technol Health Care 2018; 26: 329-341.
[20] Shen Z, Fan Y, Zhang X, Han Z and Wei C. Design and testing of a pressure measurement and adjustment device for fracture ends. Zhongguo Yi Liao Qi Xie Za Zhi 2024; 48: 335-338.
[21] Xie H, Cao L, Ye L, Du J, Shan G, Hu J, Jiang C and Song W. Autogenous bone particles combined with platelet-rich plasma can stimulate bone regeneration in rabbits. Exp Ther Med 2020; 20: 279.
[22] Leung KS, Shi HF, Cheung WH, Qin L, Ng WK, Tam KF and Tang N. Low-magnitude high-frequency vibration accelerates callus formation, mineralization, and fracture healing in rats. J Orthop Res 2009; 27: 458-465.
[23] Goodship AE, Lawes TJ and Rubin CT. Low-magnitude high-frequency mechanical signals accelerate and augment endochondral bone repair: preliminary evidence of efficacy. J Orthop Res 2009; 27: 922-930.
[24] Lv J, Qi W and Leung FKL. Advancements in micromotion-based fixation systems for fracture healing. J Orthop Surg (Hong Kong) 2025; 33: 10225536251352559.
[25] Jantorn P, Noosak C, Iamthanaporn K and Saeloh Sotthibandhu D. Silk fibroin thermosensitive polymers: osteogenic, anti-inflammatory, and angiogenic effects for osteomyelitis treatment. J Biomater Sci Polym Ed 2026; 37: 1-17.
[26] Yu T, Ding Q, Wang N, Zhang S, Cheng Z, Zhao C, Li Q, Ding C and Liu W. Cranial repair-promoting effect of oxidised sodium alginate/amino gelatine injectable hydrogel loaded with deer antler blood peptides. Int J Biol Macromol 2025; 305: 141116.
[27] Barcik J, Ernst M, Buchholz T, Constant C, Mys K, Epari D, Zeiter S, Gueorguiev B and Windolf M. Bone formation between 2.5 and 25% interfragmentary strain induced by immediate and delayed loading in a bone healing model with a monotonic strain gradient. Ann Biomed Eng 2025; [Epub ahead of print].
[28] Ghimire S, Miramini S, Richardson M, Mendis P and Zhang L. Role of dynamic loading on early stage of bone fracture healing. Ann Biomed Eng 2018; 46: 1768-1784.